Proceedings of
ASME TURBO EXPO 2002
June 3-6, 2002, Amsterdam, The Netherlands

GT-2002-30111

PERFORMANCE EVALUATION OF GAS TURBINE-FUEL CELL HYBRID MICRO GENERATION SYSTEM

Shinji Kimijima and Nobuhide Kasagi

The University of Tokyo
Department of Mechanical Engineering
Hongo 7-3-1, Bunkyo-ku, Tokyo, 113-8656, Japan

ABSTRACT

Design-point and part-load characteristics of a gas turbine-solid oxide fuel cell hybrid micro generation system, of which total power output is 30 kW, are investigated for its prospective use in the small distributed energy systems. A cycle analysis of the hybrid system has been performed to obtain general strategies of highly efficient operation and control. The method of analysis has been compared with previous results, of which power output values are set in the range from 287 to 519 kW. Then, the part-load performance of the 30 kW system has been evaluated. Two typical operation modes, i.e., constant and variable rotation speed gas turbine operation are considered. It is found that the variable speed mode is more advantageous to avoid performance degradation under part-load conditions. Operating under this mode, despite of 10 % adiabatic efficiency drop in the gas turbine components, the generation efficiency can be maintained over 60 % (LHV) in the power output range from 50 to 100 %.

NOMENCLATURE

C	heat-capacity ratio		F	Faraday constant	C/mol
G	Gibbs energy	J/kg	H	enthalpy flow	W
J	current density	A/ m^2	K	equilibrium constant	
N	rotation speed	1/s	Q	heat flow	W
R	gas constant	J/mol K	T	temperature	K
U	utilization factor		V	voltage	V
W	power	W	m	mass flow rate	kg/s
n	mole number	mol	p	pressure	atm
u	tip speed	m/s	x	mole fraction	
δ	thickness	m	η	efficiency	
ρ	resistivity	Ω m	NTU	number of heat transfer unit	

Subscripts

cell	: SOFC cell	ref	: reforming or reference
shf	: shifting	an	: anode
ca	: cathode	el	: electrode
net	: net value	act	: activation polarization
r	: recuperator	c	: compressor
t	: turbine	DA	: inverter
gcfc	: gas compressor (SOFC)	gcgt	: gas compressor (μGT)
blow	: blower	gen	: generator
SOFC	: solid oxide fuel cell	gt	: gas turbine
in	: inlet	out	: outlet
DP	: design point		

1. INTRODUCTION

Small distributed generation systems are expected to achieve highly effective energy utilization. Currently, micro gas turbines (μGT) [1] under 100 kW are rapidly spreading in the power generation market. In addition, a concept of much smaller μGT, of which power output is 5 kW, was suggested [2]. Micro gas turbines have a perspective to achieve much higher efficiency as 40 % by introducing a higher turbine inlet temperature (TIT) and higher recuperator effectiveness [3]. However, achievement of much higher efficiency than 40 % with traditional μGT is crucially difficult, while a μGT combined with a solid oxide fuel cell (SOFC) is expected to attain extremely higher efficiency. It has been indicated that μGT-SOFC hybrid systems offer efficiency over 70 % [4], and it is reported that trial operation of a hybrid system, of which power output is 220 kW, was launched [5, 6]. This study was initiated to establish a strategy to develop much smaller systems to meet increasing energy demands in commer-

cial sectors such as small businesses. As the first step, a design strategy of a 30kW hybrid system was investigated and its conceptual design was reported [7].

Recently, several hybrid system configurations have been suggested for efficiency improvement. In addition, performance prediction under part-load conditions has been made for the systems, of which power output is over 200 kW [8, 9, 10]. Among them, Magistri et al. [11] proposed a very small gas turbine (5 kW) combined with a SOFC (31 kW), and evaluated its part-load performance.

In this paper, design-point and part-load performance of a 30 kW hybrid system is investigated to find a strategy for highly efficient operation by a presently developed simulation code. A cycle analysis method which includes an empirical part-load characteristic of a small gas turbine is described, and calculation results of a 300 kW hybrid system are compared with the previously reported ones to verify the present analysis method . Performance of a 30 kW hybrid system under two different part-load operation modes, i.e., constant and variable rotation speeds of a gas turbine, are explored. In addition, effect of an operating curve, which gives a relationship between pressure ratio and mass flow rate of a working fluid, on generation efficiency is investigated under a variable speed mode.

2. SYSTEM CONFIGURATION AND CYCLE ANALYSIS METHOD

2.1 System configuration

Figure 1 shows a schematic diagram of a μGT-SOFC hybrid system. This system is based on a conventional recuperative gas turbine cycle with a SOFC as a topping component. The combustor is equipped to completely oxidize residual species included in the anode exhaust gas. This system is fed with methane at an atmospheric temperature and pressure. The reference data in Fig. 1 are extracted from our conceptual design in the best possible case [7].

In this system, the air compressed and preheated is supplied into the cathode of the SOFC. Oxygen in the cathode outlet air is exploited to burn residual hydrogen, carbon oxide and methane in the anode outlet gas. The effluent from the combustor is expanded in the turbine, and then used in the recuperator to preheat the intake air. In the reformer, methane is pre-reformed with the steam in the anode effluent and the excess heat from the power generation process in the SOFC.

2.2 Modelling approach

The present analysis is intended to evaluate overall performance of a μGT-SOFC hybrid system. A thermodynamic cycle analysis of a recuperative gas turbine coupled with an equilibrium calculation of a SOFC is established to predict design-point and part-load performance. We consider mass and energy balance equations for energy conversion processes in all components. Temperatures, pressures and compositions of a working gas at the inlet/outlet of each component are also concerned. Component models are independent of their specific factors, i.e., struc-

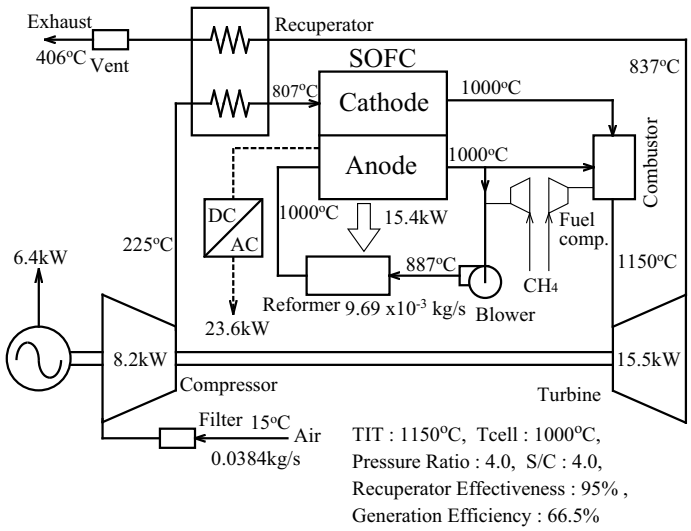

Fig. 1 Schematic diagram of μGT-SOFC hybrid system

Table 1 Basic calculation condition

	30kW	300kW
Cell Temperature (°C)	1000	900
Turbine Inlet Temperature (°C)	1150	1100
Pressure Ratio (-)	4.0	3.5
Recuperator Temperature Effectiveness (%)	95	85
Compressor Adiabatic Efficiency (%)	73	76
Turbine Adiabatic Efficiency (%)	80	86
GT Mechanical Efficiency (%)	95	
Blower Adiabatic Efficiency (%)	70	
Blower Mechanical Efficiency (%)	90	
Gas Compressor Adiabatic Efficiency (%)	60	
Gas Compressor Mechanical Efficiency (%)	90	
Steam Carbon Ratio (-)	4.0	3.0
Current Density (A/m^2)	3000	
H_2 Utilization Ratio (%)	80	
Cathode Thickness (mm)	2	
Anode Thickness (mm)	0.1	
Electrolyte Thickness (mm)	0.02	
SOFC Pressure Drop (%)	5	
Reformer Pressure Drop (%)	4	
Filter Pressure Drop (%)	0.5	
Vent Pressure Drop (%)	0.5	
Recuperator Pressure Drop (Air Side) (%)	3	
Recuperator Pressure Drop (Exhaust Side) (%)	2	
Atmospheric Temperature (°C)	15	
Generator Efficiency (%)	98	
Inverter Efficiency (%)	93	

tures of a compressor and turbine, a cell geometry, a stack configuration and a type of a reformer. Theoretical expressions are introduced into the cycle analysis to indicate general characteristics of components. However, empirical relationships developed in previous studies are employed to estimate part-load characteristics of a gas turbine and a voltage drop in a SOFC.

2.3 Assumptions for cycle analysis

In the present work, following assumptions are employed to simplify the cycle analysis method.

(1) Steady state operation is considered.

(2) Gases do not leak outside the system.

(3) Heat loss is negligibly small.

(4) Relative pressure loss remains constant.

(5) Chemical reaction proceeds to an equilibrium state.

(6) Internal distribution of a temperature, a gas composition and a pressure in each component is not taken into account.

(7) The heat for the fuel reforming is supplied from the cell.

(8) Temperatures of the anode outlet, cathode outlet and reformer outlet are all equal to the cell temperature.

(9) In the combustion chamber, the residual chemical species from the anode and injected methane are burnt completely.

Thermodynamic and chemical properties of working fluids are based upon the JANAF tables [12], except methane [13].

2.4 Micro Gas Turbine

2.4.1 Power output

In calculations of compression and expansion processes, outlet conditions from a compressor and turbine are estimated by assuming an isentropic path and then applying appropriate efficiency to determinate an actual outlet condition for a given set of an inlet condition. Adiabatic efficiency (same as "isentropic efficiency") is exploited to evaluate irreversibility in the compressor and turbine, so that we can obtain the actual outlet enthalpy. Taking into account the power consumption in the fuel gas compressor and efficiency of the rotating components, the power output of the gas turbine can be obtained by the following equation:

$$W_{gt} = \eta_{gen}\left(\eta_{gt} W_t - W_c\right) - W_{gcgt}. \qquad (1)$$

2.4.2 Recuperator effectiveness

During part-load operation, the heat transfer area is unchanged, thereby the temperature effectiveness is changed with the flow rate of the working fluid. However, the Nusselt number is assumed to be constant under the following assumptions:

- the fluid flow in the recuperator is laminar,
- the thermal conductivity of working fluid is constant.

In our previous work [7], the values of the Reynolds number at the design-point are estimated 216 for the air flow and 214 for the combustion gas flow, respectively. Based on these, the overall heat transfer coefficient becomes constant. As a result, the temperature effectiveness of the recuperator in counterflow arrangement η_R can be estimated as follows [14] :

$$\eta_R = \frac{1 - \exp\left[\left(C_r - 1\right)\mathrm{NTU}\right]}{1 - C_r \exp\left[\left(C_r - 1\right)\mathrm{NTU}\right]}, \qquad (2)$$

$$\mathrm{NTU} = K_r A_r \Big/ \left(m_{air} c_{pair}\right), \qquad (3)$$

$$C_r = m_{air} c_{pair} \Big/ \left(m_{cg} c_{pcg}\right), \qquad (4)$$

where K_r is the overall heat transfer coefficient, A_r is the heat transfer area, m_{air} is the air mass flow rate, c_{pair} is the air specific heat, m_{cg} is the combustion gas mass flow rate, and c_{pcg} is the combustion gas specific heat, respectively.

2.4.3 Rotation speed

To estimate a rotation speed of the radial turbine, its peripheral speed, u, should be calculated. This is estimated by the following approximation based on a frequently used guideline [14]:

$$u \approx 1.1\sqrt{\Delta h_0}\ , \qquad (5)$$

where Δh_0 is the stagnation enthalpy change in the turbine. Then, the rotation speed can be estimated as follows:

$$N / N_{\mathrm{DP}} = \sqrt{\Delta h_0 / \Delta h_{0\mathrm{DP}}}\ . \qquad (6)$$

2.5 Solid Oxide Fuel Cell

2.5.1 Reformer

In the reformer, hydrogen and carbon oxide are produced from methane and steam. The reforming/shifting reaction below are assumed.

$$\text{Reforming:} \quad \mathrm{CH_4 + H_2O \rightarrow 3H_2 + CO} \qquad (7)$$

$$\text{Shifting:} \quad \mathrm{CO + H_2O \rightarrow H_2 + CO_2} \qquad (8)$$

Reforming and shifting processes proceed simultaneously. Heat absorbed into reforming reaction is greater than released heat from shifting reaction. Then, overall reaction in a reformer is endothermic.

The heat required for the overall reforming reaction Q_{ref} can be obtained from energy flows into and out of the reformer. The steam/carbon ratio, S/C, is defined as the mole fraction of steam in the recirculated anode exhaust gas to supplied methane as:

$$\mathrm{S/C} = n_{\mathrm{H2O}} / n_{\mathrm{CH4}}\,. \qquad (9)$$

2.5.2 Nernst voltage

In the cell, hydrogen and carbon oxide react, and the electric power is simultaneously generated through the following electrochemical oxidation processes:

$$\text{Hydrogen:} \quad \mathrm{H_2 + 1/2O_2 \rightarrow H_2O} \qquad (10)$$

$$\text{Carbon oxide:} \quad \mathrm{CO + 1/2O_2 \rightarrow CO_2} \qquad (11)$$

In the present analysis, reaction in the SOFC is assumed to proceed to the equilibrium state. Using ΔG_{H2} , which represents the change of the Gibbs energy before and after the reaction of hydrogen, the Nernst voltage is obtained as follows:

$$V_{\mathrm{H2}} = -\frac{1}{2F}\Delta G_{\mathrm{H2}} - \frac{RT}{2F}\ln\left(\frac{p_{an,\mathrm{H2O}}}{p_{an,\mathrm{H2}}\sqrt{p_{ca,\mathrm{O2}}}}\right). \quad (12)$$

Equation (12) can be transformed into the following expression by using the equilibrium constant K_{H2} and mole fractions.

$$V_{\mathrm{H2}} = \frac{RT}{2F}\left\{\ln K_{\mathrm{H2}} - \ln\left(\frac{x_{an,\mathrm{H2O}}}{x_{an,\mathrm{H2}}}\right) + \frac{1}{2}\ln\left(x_{ca,\mathrm{O2}}p_{ca}\right)\right\}. \quad (13)$$

Currently, there are uncertainty and arguments whether electrochemical oxidation of carbon oxide proceed in the SOFC or not. However, in the present analysis, we assume that carbon oxide is electrochemically oxidized in the anode [15]:

$$V_{\mathrm{CO}} = \frac{RT}{2F}\left\{\ln K_{\mathrm{CO}} - \ln\left(\frac{x_{an,\mathrm{CO2}}}{x_{an,\mathrm{CO}}}\right) + \frac{1}{2}\ln\left(x_{ca,\mathrm{O2}}p_{ca}\right)\right\}. \quad (14)$$

Reaction heat is obtained from the data of the formation enthalpy in JANAF table [12], except methane [13]. Using these fundamental data, the Gibbs energy can be calculated. Then the equilibrium constants are obtained from the Gibbs energy, the universal gas constant and the reaction temperature.

The fuel and oxygen utilization factor are defined as follows, respectively:

$$U_{\mathrm{H2}} = n_{\mathrm{H2,consumed}}/n_{\mathrm{H2,supplied}}, \quad (15)$$

$$U_{\mathrm{O2}} = n_{\mathrm{O2,consumed}}/n_{\mathrm{O2,air}}. \quad (16)$$

It is assumed that the reaction amount of carbon oxide is determined to satisfy V_{H2}=V_{CO} [7].

2.5.3 Overpotential

In an actual cell, the net voltage is usually lower than the Nernst voltage due to overpotential of activation, concentration and ohmic polarization. It is assumed that the effect of the concentration polarization is negligibly small against the effects of the other polarization. This assumption is considered to work well, because diffusions of reactants through electrodes are sufficiently fast under high temperature operation [8]. The activation overpotential is estimated by the previously suggested approximation of the Butler-Volmer's equation reported by Nagata et al. [16]. The resistivity of the cell component materials can be calculated by the equations developed by Bessette et al. [17].

2.5.4 SOFC power output

Considering the activation overpotential and ohmic loss, the net voltage of the cell is calculated as:

$$V_{net} = V_{\mathrm{H2}} - V_{act} - J_e\left(\rho_{an}\delta_{an} + \rho_{ca}\delta_{ca} + \rho_{el}\delta_{el}\right). \quad (17)$$

The generated current is directly obtained from the amount of the reaction species. The power output of the SOFC, W'_{SOFC}, is calculated from the net voltage and current. The efficiency of the power conditioning unit and the power for the SOFC auxiliaries, i.e., the fuel compressor and anode gas recirculation blower should be considered. Thus, the net power output is obtained as follows:

$$W_{SOFC} = \eta_{DA}W'_{SOFC} - W_{gcfc} - W_{blow}. \quad (18)$$

2.5.5 SOFC energy balance

From the total inlet enthalpy H_{in} and the reaction enthalpy change ΔH_{cell}, the total cell exit enthalpy H_{out} is obtained as:

$$H_{out} = \left[H_{in} + \left(-\Delta H_{cell}\right)\right] - \left(W'_{SOFC} - Q_{ref}\right). \quad (19)$$

Assuming that the anode and cathode outlet temperatures are equal, they are obtained from H_{out}. We can derive the fuel consumption in the SOFC for a certain cell temperature by iterative calculations. Part of the anode exit gas is recirculated and exploited to supply the reforming reaction with steam. The flow rate of recirculated gas is determined from the required S/C ratio.

2.6 Overall System Efficiency

In the present analysis, based upon the total power output and the total energy input estimated from the lower heating value of methane ΔH_{CH4} , the power generation efficiency of the overall system η_{sys} is defined as follows:

$$\eta_{sys} = \frac{W_{gt} + W_{SOFC}}{\left(m_{gt} + m_{SOFC}\right)\Delta H_{\mathrm{CH4}}}. \quad (20)$$

3. COMPARISON WITH PREVIOUS ANALYSES

3.1 Design-point analysis

As a preliminary assessment of the cycle analysis method, the design-point performance is discussed in this subsection. The cycle analysis with respect to a 300 kW hybrid system, of which configuration is represented in Fig. 1, is performed with calculation input specified in Table 1. An example of the calculation results, i.e., temperatures at the relevant cycle points and the energy conversion in each component are shown in Fig. 3.

Under the design-point condition, the generation efficiency is expected to be nearly 63 %. The turbine outlet temperature seems to be high (798 °C) for an ordinary metallic recuperator because of the high TIT (1100 °C). However, in the Japanese ceramic gas turbine R&D program [18], it is reported that a plate-fin type metallic recuperator can be operated at 832 °C.

Earlier work done by other workers and present results, of which power output values are set in the range from 287 to 519 kW, are summarized in Table 2. This range of the total power output is selected as a distributed power generation application. The Conditions of pressure ratio are set to be approximately 3.0~3.5. The operating temperatures of the SOFC is around 900 °C. The results of overall efficiency fall in the range from 57 to 65%, and the power output ratio of μGT to the total is around

15~30 %. These minor disagreement are considered due to the different system configurations and calculation input, i.e., current density, adiabatic efficiency, TIT and so on, so that the present analysis method should be equivalent to those developed by other workers.

3.2 Part-load analysis

Recent advancement in a field of power electronics devices has made it possible to precisely control power output of an electric generator. This progress enables us to apply variable speed control technique to gas turbine operation. In the previous work [8, 9, 10, 11], variable speed technique is considered to obtain even more efficient operation of hybrid systems.

Performance prediction of small turbomachines with solely mathematical and physical description is difficult, and empirical knowledge should be exploited in any system simulation. In the most of previous work [8, 9, 10], generic maps of existing compressor and turbine were employed to estimate performance of a small gas turbine. On a compressor map, a stable operating line can be obtained as combined characteristics of a compressor and other downstream components. Tracing this line, a performance curve of a gas turbine under part-load conditions can be predicted.

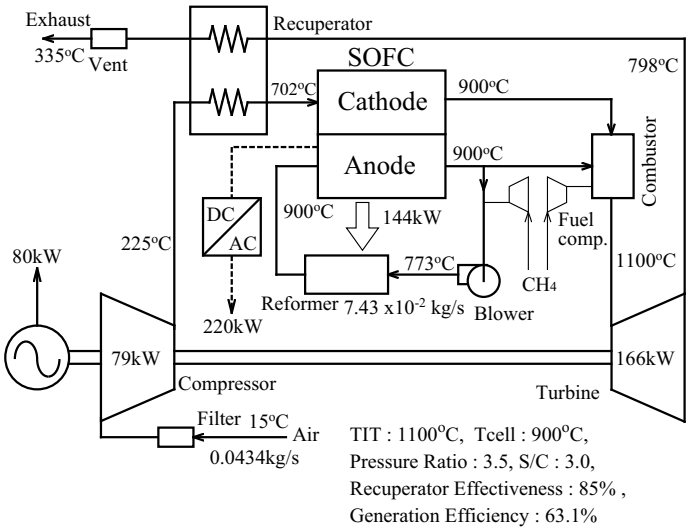

Fig. 3 Example of calculation result of 300 kW hybrid system under design-point condition

This evaluation method is also employed in the present work.

From the above requirement, the operating line on the compressor map discussed in previous work [9] is introduced into the present analysis. Figure 4 represents the operating line, and (I) is the so-called standard line [9]. The corrected mass flow rate m_r is defined as follows:

$$m_r = m_c\left(P_{ref}/P\right)\sqrt{T/T_{ref}}\,, \tag{21}$$

where m_c is the air flow rate, and T, P are the suction temperature and pressure, respectively. On the other hand, instead of the pressure ratio, the corrected enthalpy change Δh_r is used. Its definition is given as follows:

$$\Delta h_r = \Delta h_{re}\Big/\left(c_{p0}T_{ref}\right), \tag{22}$$

where c_{p0} is the specific heat at the ambient temperature, and Δh_{re} is the real enthalpy change. In Eqs. (21) and (22), the reference temperature T_{ref} and pressure P_{ref} are fixed at 288.15 K and 101.325 kPa, respectively.

In addition to the above, two pairs of adiabatic efficiency are assumed as shown in Table 3. The cases (A) and (B) are the design condition and assumption of 10% degradation, respectively. If the adiabatic efficiency degradation is kept within 10 %, the part-load operating point stays in the region between two performance curves of (A) and (B).

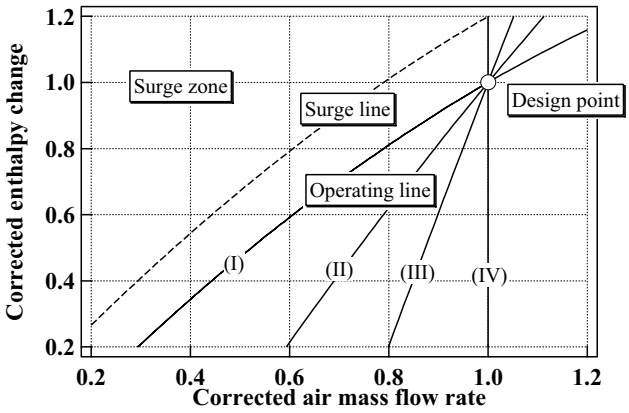

Fig. 4 Combined characteristics of compressor and downsteam components on compressor performance map

Table 2 Comparison of design-point performance

Author		Veyo et.al [6]	Costamagna et.al [8]	Campanari [9]	Palsson and Selimovic [10]	Present work
Power output kW	Total	307	287	259	519	300
	SOFC	251	241	207.8	348	220
	μGT	67	46	53.2	171	80
Pressure ratio	Turbine	-	3.15	3.06	3.5	3.5
	Compressor	3.5	3.89	3.81	-	3.95
TIT °C		872	900	900	885	1100
Efficiency (LHV)		57.0	61.1	64.9	64.2	63.1

The part-load performance of the SOFC is considered to depend on the voltage drop caused by polarization. The net voltage can be estimated by Eq. (17), and we can understand that the smaller current density gives the smaller voltage drop. The current is determined by the energy balance of the SOFC based upon its operating conditions, i.e., the electrical load, the fuel flow rate, the operating temperature and pressure. Since the effective cell area is assumed to be constant, the current density is reduced in proportional to the current. Under part-load conditions, the electrical performance of the SOFC is theoretically improved by the reduction of the current density.

As the fuel flow rate decreases, the SOFC must be able to oxidize more fuel, i.e., the fuel utilization should be increased at a lower load. However, the investigation of the electrochemical reaction kinetics in the SOFC is beyond the scope of this paper, hence it is assumed that the fuel utilization factor is kept constant at 0.80 during part-load operation.

Regarding auxiliaries such as the fuel compressor and the anode gas recirculating blower, their adiabatic and mechanical efficiency are fixed at the design values. Likewise, energy conversion efficiency of the generator, the inverter and the DC/AC converter are assumed to be constant at the design-point values.

In Fig. 5 (a), in the partial output range from 80 to 100 %, the

Table 3 Condition of component effciency

	(A)	(B)
Compressor adiabatic efficiency	76.0%	68.4%
Turbine adiabatic efficiency	86.0%	77.4%
Recuperator temperature effectiveness	85.0% (design point)	

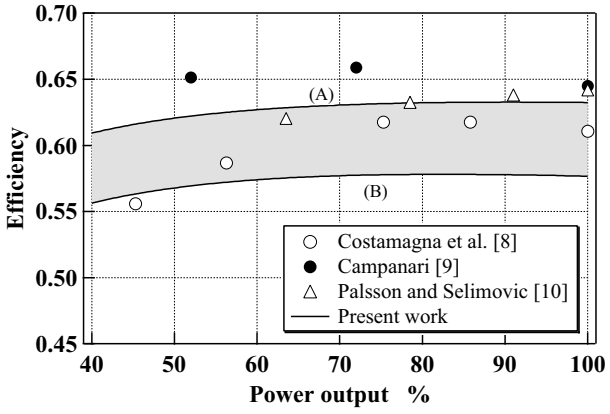

(a) Power generation efficiency

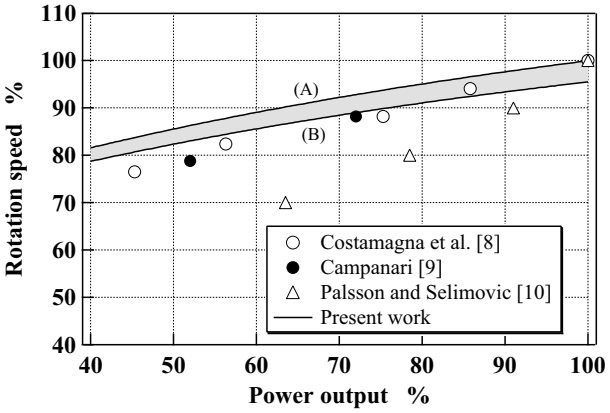

(b) Rotation speed ratio

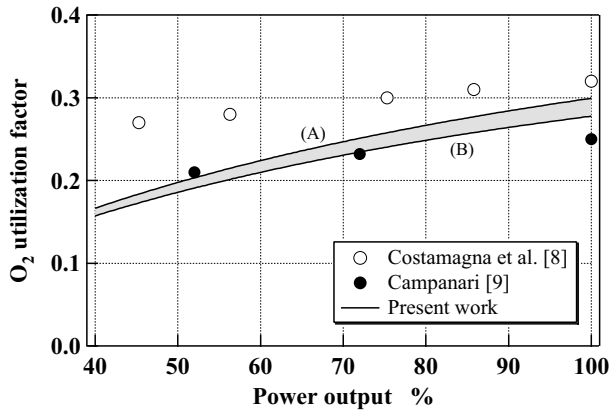

(c) Oxygen utilization factor

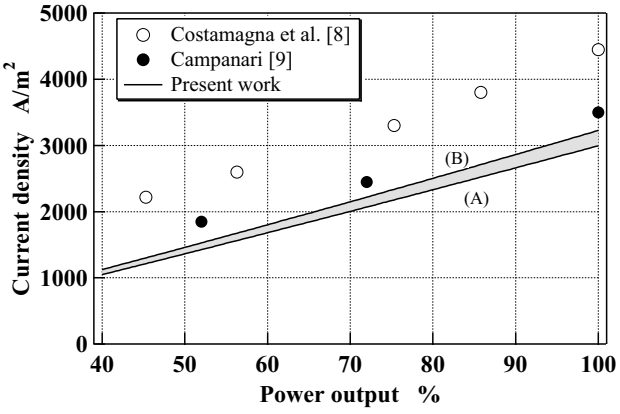

(d) Current density

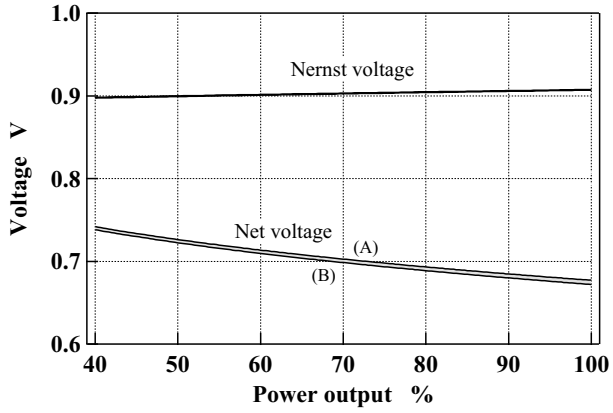

(e) Cell voltage

Fig. 5 Estimated part-load characteristics of 300kW μGT-SOFC hybrid system

generation efficiency estimated in the previous work of Costamagna et al. [8] and Campanari [9] slightly increase with decreasing electrical load, whilst the present result remains almost constant efficiency. This seems to be caused by the synergistic effect of the following factors:

- the reduction of the voltage drop,
- the improvement of the recuperator effectiveness,
- the component efficiency degradation except the recuperator.

Below 80 % partial load, the generation efficiency is decreased together with the power output. The degradation rate of present result is smaller than the estimation of Costamagna et al. [8]. This difference is probably due to the different system configurations and operating conditions.

Figure 5 (b) shows the relation between the electrical load and the rotation speed, the latter of which is estimated by Eq. (6). The change of the rotation speed is limited by the operating line. It is found that the result of Palsson and Selimovic [10] has a larger reducing rate against the other results. This noticeable difference in the rotation speed is believed to be due to the different characteristic maps of the compressor and turbine.

Figure 5 (c) shows the variation of the oxygen utilization factor in the cathodic electrode. The estimates in the present work are similar to the previous ones in spite of assuming the different fuel utilization factors. This means that the ratio of the air flow rate to the fuel consumption is almost comparable among all the cited results.

The variation of the current density is shown in Fig. 5 (d). The present design-point value (3000 A/m^2) is the smallest among the three cases, and all present values are substantially smaller than those of Costamagna et al. [8]. Figure 5 (e) shows the estimated cell voltage in the present work. It is found that the Nernst voltage is around 0.9 V at the design point. Likewise, the net voltage is estimated to be around 0.67 V. This level is in an agreement with a recent SOFC technology [19]. Under part-load conditions, the theoretical voltage seems to be slightly decreased together with the pressure ratio, whereas the net voltage is increased by the reduction of the current density.

4. PERFORMANCE EVALUATION OF 30 KW HYBRID SYSTEM AT PART-LOAD OPERATION

4.1 Calculation condition

In this subsection, part-load characteristics of the 30 kW hybrid system, which is conceptually designed in our previous work [7], are discussed. Two typical operation modes, i.e., constant and variable speed operation, are taken into account. Calculation conditions of all the components are fixed at each design-point value summarized in Table 1, and the operating line (I) cited in Fig. 4 is employed in the present analysis. The adiabatic efficiency of the compressor and turbine under the variable speed operation are assumed to be constant in two cases of the design-point and 10 % degradation as shown in Table 4.

Table 4 Condition of component efficiency

	(A)	(B)
Compressor adiabatic efficiency	73.0%	65.7%
Turbine adiabatic efficiency	80.0%	72.0%
Recuperator temperature effectiveness	95.0% (design point)	

The design-point efficiency of the present system indicated in Fig. 1 is much higher than that of the previous result discussed by Magistri et al. [11], because the present analysis is based on the best possible component performance to be achieved in the future, i.e., T_{cell} = 1000 °C , TIT = 1150 °C and η_R = 95 %. Table 5 shows the calculation result of the anode inlet gas composition at the design point. The residual methane ratio is kept to be sufficiently small due to the high reforming temperature.

4.2 Results and discussions

In order to keep the rotation speed constant, the pressure ratio and TIT should be maintained to be constant during the part-load operation (Fig. 6 (a)), since the rotation speed depends on the enthalpy drop in the turbine. In this case, the power output of the μGT is almost constant (Fig. 6 (b)); namely, this operation is regarded as a constant μGT power operation. Then, the total power output is solely regulated by the SOFC power output. Under the variable speed conditions, the pressure ratio is changed along the operating line. Thus, the rotation speed is decreased with decreasing power output (Fig. 6 (c)), and it reaches around 85 % of the design-point value at 50 % partial load.

In Fig. 6 (d), assuming the constant adiabatic efficiency of the compressor and turbine, the variable speed mode offers the almost constant generation efficiency. Note that it is maintained over 60 % (LHV) in the power output range from 50 to 100 %. In contrast, the generation efficiency of the constant speed mode is reduced with decreasing power output. These noticeable differences are considered to be due to the operating condition of the SOFC, i.e., the operating temperature reduction.

Under the constant speed operation, the reduction of the SOFC fuel input leads to the decrease of the cell stack temperature as shown in Fig. 6 (e). Despite of the fuel reduction, the constant speed operation gives the almost constant suction air flow rate and pressure ratio, and thereby the cell stack temperature is decreased to satisfy the energy balance provided by the expression (19). As shown in Fig. 6 (f), this results in the fact that the combustor fuel input should be increased to elevate the temperature of the SOFC effluent to the targeted TIT (1150 °C). Similarly, the oxygen utilization factor of the constant speed is smaller than that of the variable speed as also shown in Fig. 6 (e). This means that the air is excessively supplied to the cathode and its amount is unsuitable to the fuel input. The above mentioned fact is likely one of the major reasons for the generation efficiency reduction. It is pointed out that the cell stack temperature

Table 5 Example of anode inlet gas compsition

Temp. °C	Pressure kPa	Mole fraction %							
		N_2	O_2	Ar	CO_2	CO	H_2	H_2O	CH_4
943.5	460.3	0.00	0.00	0.00	14.36	18.97	32.21	34.45	0.01

strongly affects the performance of the fuel reforming process. The excessive temperature drop of the cell stack leads to the incomplete internal reforming.

On the other hand, under the variable speed operation, the cell stack temperature can be kept constant at the full load value. The additional fuel into the combustor is held quite small. As a result, under the part-load conditions, the generation efficiency of the variable speed is higher than that of the constant speed.

As described above, the performance degradation under the constant speed conditions should be due to the temperature drop of the cell stack. Being associated with this, the overpotential is simultaneously increased. However, as the data in Fig. 6 (g) indicate, the net voltage is maintained at the same level as expected from the constant cell stack temperature, since the theoretical voltage is significantly increased with decreasing cell stack temperature.

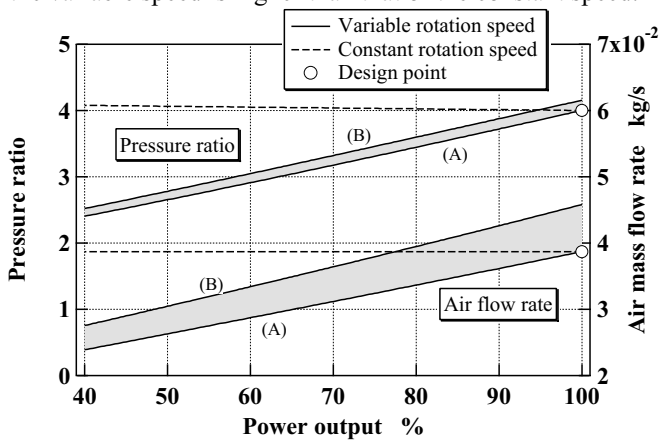

(a) Pressure ratio in turbine and air mass flow rate

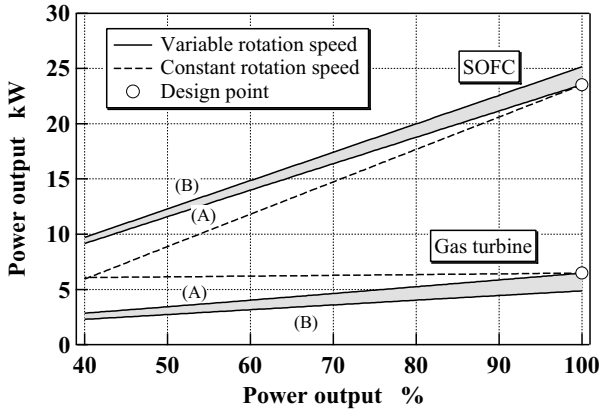

(b) Power output of μGT and SOFC

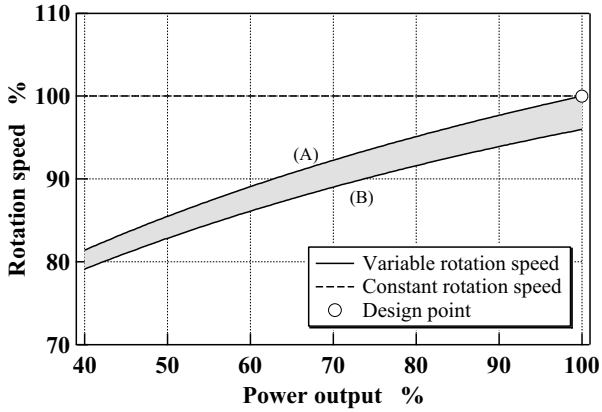

(c) Rotation speed ratio

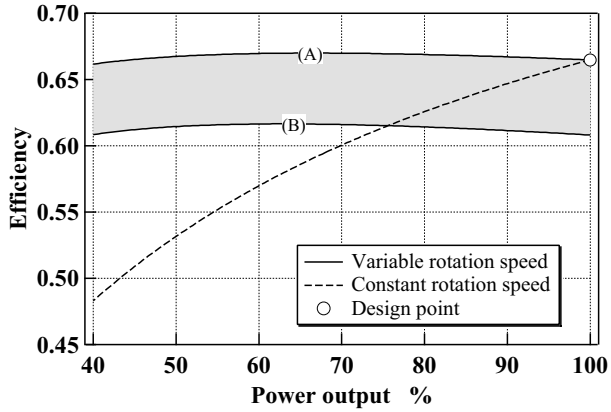

(d) Power generation efficiency

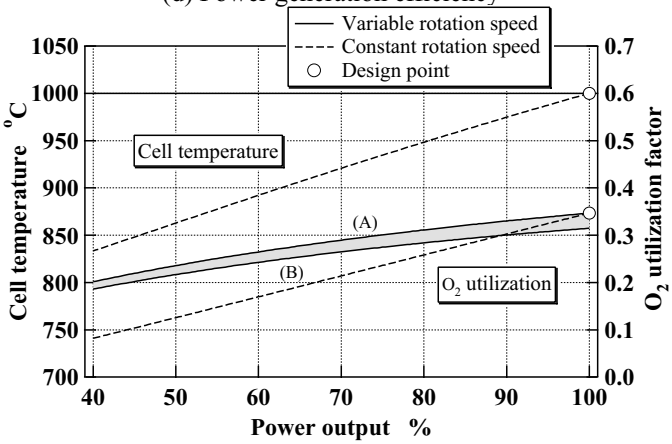

(e) Cell stack temperature and oxygen utilization factor

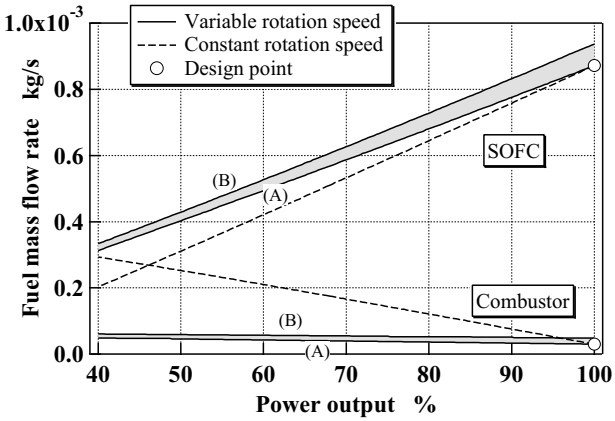

(f) Fuel input

Fig. 6 Part-load characteristics of 30kW hybrid system

The turbine outlet temperature are shown in Fig. 6 (h). Under the variable speed operation, the turbine exhaust temperature is increased with decreasing power output due to the reduction of the pressure ratio (Fig. 6 (a)). From a view point of thermal endurance, a materials selection of a recuperator [20] is a difficult issue for actual variable speed operation.

Figure 6 (i) shows the temperature and mass flow rate of the combustion gas discharged from the hybrid system. Under the constant speed operation, the exhaust temperature is kept around 300 °C, and the flow rate is also nearly constant. These characteristics result from the constant pressure ratio and TIT. Under the variable speed operation, the exhaust temperature and flow rate are simultaneously reduced with decreasing power output. The temperature is decreased to under 250 °C at 50 % of the total power output. In the latter case, the flow rate of the working fluid is significantly decreased with the load reduction. Then, in the recuperator, the heat recovery from the turbine effluent is increased, because the recuperator effectiveness is improved by the reduction of the air flow rate. Thus, the temperature of discharged gas is decreased together with the power output. However, in both cases, the temperature levels are high enough for hot-water supply, space heating and cooling in commercial sectors.

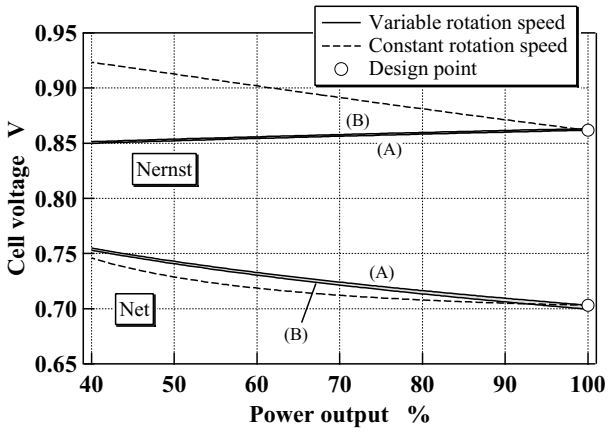

(g) Theoretical and net cell voltage

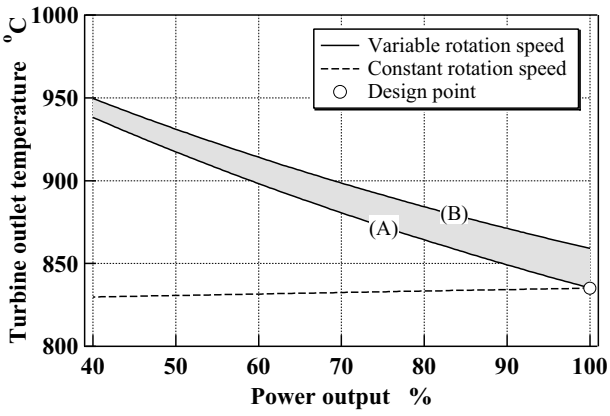

(h) Turbine outlet temperature

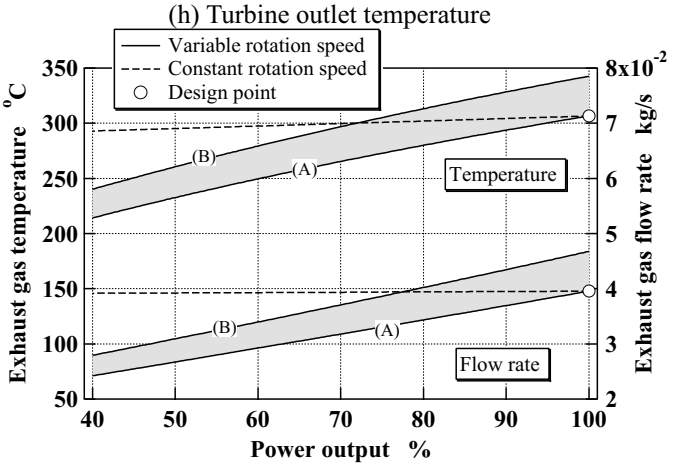

(i) Exhaust gas temperature and flow rate

Fig. 6 Part-load characteristics of 30kW hybrid system

4.3 Effects of operating line

In this subsection, the effect of the operating line on the system performance is explored. Figure 7 shows the part-load characteristics obtained by using the operating lines depicted in Fig. 4. The compressor and turbine adiabatic efficiency are fixed at each design-point value, respectively. The line (I) represents the performance criterion, whilst the line (IV) is based on the constant air mass flow rate condition. Approaching the constant flow rate line of (IV), namely the operating condition closes to that of the constant speed mode, the system performance is deteriorated. In other words, the smaller flow rate condition provides much higher efficiency under the same pressure ratio (Fig. 4). The effect of this characteristics is emphasized under the even more smaller power output. However, keeping the pressure ratio constant with decreasing flow rate, the operating point approaches the surge line.

The stable compressor operation is possible only in the region below the compressor surge line shown in Fig. 4. While the operating line is separate from the surge line, the operating point can be temporarily in the surge region during an acceleration period. A small gas turbine and its control system must be developed to avoid a surge with a sufficient design margin. For this purpose, it will be mandatory to establish an analysis method of dynamic behavior of hybrid systems.

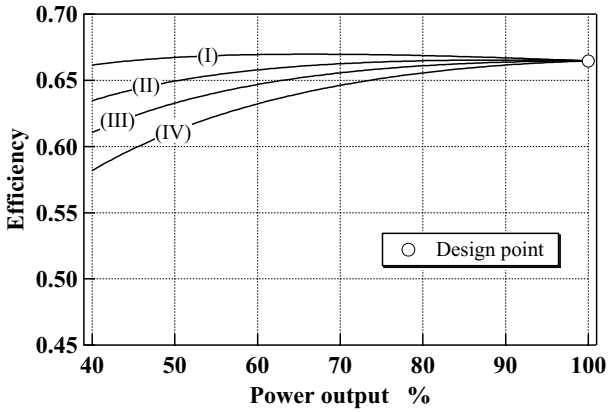

Fig. 7 Effect of operating line on generation efficiency

5. CONCLUSIONS

Performance evaluation of a μGT-SOFC hybrid system including part-load operation is made in the present work. The following major conclusions are derived:

(1) A cycle analysis method is verified by favorable comparison of our results with the others in the literature. The present analysis method has sufficient capability to evaluate performance of hybrid systems under various partial conditions.

(2) The part-load performance of a 30kW hybrid system, which was conceptually designed, is predicted. Under the part-load conditions, the variable speed operation is superior to the constant speed operation. While the adiabatic efficiency of the gas turbine components is by 10 % degraded, the variable speed operation has the potential to keep the generation efficiency over 60 % (LHV) in the power output range from 50 to 100 %. By using a higher temperature recuperator, a variable speed mode is recommended as a strategy for high performance part-load operation. However, it is noted that exhaust heat of constant speed operation is more adequate for thermal energy supply.

(3) An operating line, namely a matching condition of a compressor and other downstream components, significantly affects system performance. System efficiency is increased when approaching a surge region. However, operating near a surge line causes significant problems of compressor instability. The operating line should be located off a surge zone with a sufficient margin.

ACKNOWLEDGMENTS

This work was supported through the research project on "Micro Gas Turbine/Solid Oxide Fuel Cell Hybrid Cycles for Distributed Energy System" by the Department of Core Research for Evolutional Science and Technology (CREST) of the Ministry of Education, Culture, Sports, Science and Technology (MEXT).

REFERENCES

[1] Craig, P. , "The Capstone Turbogenerator as an Alternative Power Source," SAE Paper, 970292 (1997).

[2] McDonald, C. F. and Rodgers, C. , "The Ubiquitous Personal Turbine (PT)... A Power Vision for The 21st Century," ASME Paper, 2001-GT-0100 (2001).

[3] McDonald, C. F. , "Low-cost Compact Primary Surface Recuperator Concept for Microturbines," Applied Thermal Engineering, 20 (2000), 471-497.

[4] Massardo, A. F. and Lubelli, F. , "Internal Reforming Solid Oxide Fuel Cell-Gas Turbine Combined Cycles (IRSOFC-GT) : Part A - Cell Model and Cycle Thermodynamic Analysis," Trans. ASME Journal of Engineering for Gas Turbine and Power, 122 (2000), 27-35.

[5] George, A. R., "Status of Tubular SOFC Field Unit Demonstrations," Journal of Power Sources, 86 (2000), 134-139.

[6] Veyo, S. E., Shockling, L. A., Dederer, J. T., Gillett, J. E. and Lundberg, W. L., "Tubular Solid Oxide Fuel Cell/Gas Turbine Hybrid Cycle Power Systems - Status," ASME Paper, 2000-GT-550 (2000).

[7] Uechi, H., Kimijima, S. and Kasagi, N., "Cycle Analysis of Gas Turbine-Fuel Cell Hybrid Micro Generation System," ASME Paper, JPGC2001/PWR-19171 (2001).

[8] Costamagna, P., Magistri, L. and Massardo, A. F. , "Design and Par-Load Performance of a Hybrid System Based on a Solid Oxide Fuel Cell Reactor and a Micro Gas Turbine," Journal of Power Sources, 96 (2001), 352-368.

[9] Campanari, S., "Full Load and Part-Load Performance Prediction for Integrated SOFC and Microturbine Systems", Trans. ASME Journal of Engineering for Gas Turbine and Power, 122 (2000), 239-246.

[10] Palsson, J. and Selimovic, A., "Design and Off-Design Predictions of a Combined SOFC and Gas Turbine System," ASME Paper, 2001-GT-379 (2001).

[11] Magistri, L., Massardo, A., Rodgers, C. and McDonald, C. F., "A Hybrid System Based on a Personal Turbine (5kW) and a SOFC Stack: A Flexible and High Efficiency Energy Concept for the Distributed Power Market," ASME Paper, 2001-GT-92 (2001).

[12] Malcolm, W., "NIST-JANAF Thermochemical Tables Fourth Edition," Part 1 and 2, American Chemical Society & American Institute of Physics (1989) .

[13] Hougen, O. A., Watson, K. M. and Ragatz, R. A. , "Chemical process principles. part II, Thermodynamics," Appendix, John Wiley & Sons, Inc., New York (1959).

[14] Wilson, D. G. and Korakianitis, T., "The Design of High-Efficiency Turbomachinery and Gas Turbines," Second Edition, Prentice Hall (1998).

[15] Achenbach, E., "Three-dimensional and time-dependent simulation of a planar solid oxide fuel cell," Journal of Power Sources, 49 (1994), 333-348.

[16] Nagata, S., Onda, K., Momma, A., Kasuga, Y. and Kato, K., "Simulation of Temperature Dependence of SOFC and SOE," Bulletin of the Electrotechnical Laboratory (in Japanese), 57-5, 6 (1993), 598-615.

[17] Bessette, N. F., Wepfer, W. J. and Winnick, J., "A Mathematical Model of a Solid Oxide Fuel Cell," Journal of Electrochemical Society, 142-11 (1995), 3792-3800.

[18] Takehara, I., Tatsumi, T. and Ichikawa, Y., "Summary of CGT302 Ceramic Gas Turbine Research and Development Program," ASME Paper, 2000-GT-644 (2000).

[19] Singhal, S. C., "Advances in Solid Oxide Fuel Cell Technology," Solid State Ionics, 135 (2000), 305-313.

[20] Pint, B. A., Swindeman, R. W., More, K. L. and Tortorelli, P. F., "Materials Selection for High Temperature (750°-1000°) Metallic Recuperators for Improved Efficiency Microturbines," ASME Paper, 2001-GT-0445 (2001).